SPATIAL AND FREQUENCY DEPENDENCIES OF LOCAL PHOTORESPONSE OF HTS STRIP-LINE RESONATOR IN THE REGIME OF TWO-TONE MICROWAVE INTERMODULATION EXCITATION

Alexander P. Zhuravel[1], Steven M. Anlage[2], Alexey V. Ustinov[3]

[1]B. Verkin Institute for Low temperature Physics & Engineering, NAS of Ukraine
47 Lenin Avenue, Kharkov, 61103, Ukraine
Tel.: +38(057)341-0907, Fax: +38(057)340-3370, E-mail: zhuravel@ilt.kharkov.ua
[2]Center for Nanophysics and Advanced Materials, Department of Physics, University of Maryland
College Park, MD 20742-4111 USA
Tel.: (301) 405-7321, Fax: (301) 405-3779, E-mail: anlage@umd.edu
[3]Physikalisches Institut, Karlsruhe Institute of Technology (KIT)
Wolfgang-Gaede-Str. 1, D-76131, Karlsruhe, Germany
Tel.: +49-721-608-3455, Fax: +49-721-608-6103, E-mail: ustinov@physik.uni-karlsruhe.de

High-T_c superconducting (HTS) films have been widely applied in passive microwave electronics including high-Q resonators for mobile telephony. One of the crucial problems in applying such HTS devices remains their nonlinear (NL) response with respect to pumping power. This manifests itself as *global* intermodulation product distortion (IMD) when two or more high-frequency (HF) signals are NL mixed in the resonant frequency band. A predominately *local* origin of NL sources through *global* NL media motivates the development of spatially resolved methods to identify the dominant mechanisms of NL response. We have previously shown [1] that by using different imaging contrast modes of low-temperature (LT) laser scanning microscopy (LSM) one can solve this problem with great success. Additionally, a new paradigm of HF frequency-dependent singularity of LSM images was developed to spatial describe (i) local changes in surface resistance $\delta R_s(x, y)$ and (ii) HF current density distribution $J_{HF}(x, y)$ as a function of resonator (x, y) surface coordinates by using a method of spatially-resolved complex impedance partition [2]. Here, we propose a new phenomenological approach to spatially-resolved research of NL microwave properties of operating thin-film superconducting resonators. The approach is based on frequency and spatial uniqueness of LSM images that can be extracted from a set of 2-D patterns representing x-y distribution of the LSM photoresponse, $PR_f(x, y)$, at fixed third-order IMD frequencies $2f_1$-f_2 and $2f_2$-f_1 as a result of two-tone resonator microwave excitation at equidistant frequencies f_1 and f_2 relative to the fundamental resonance, f_0. We show that similar to what is described in [2] manipulation of LSM images at $2f_1$-f_2 and $2f_2$-f_1 can be used to present NL components of IMD LSM $PR(x, y)$ in terms of its independent spatial variations of (i) inductive $PR_{IMD,X}(x, y)$ and (ii) resistive $PR_{IMD,R}(x, y)$ contributions. In particular the realistic spatial coherence between such IMD components and $J_{HF}(x, y)$ flow, so crucial for determining the NL properties of the device, have not been investigated.

The tested device was a half wave YBa$_2$Cu$_3$O$_{7-\delta}$ (YBCO) microstrip (with thickness $d = 1$ μm) resonator on a 500 μm LaAlO$_3$ (ε_r=24.2) substrate (LAO) designed for operation at f_0=1.85 GHz with Q~1230 at T=78 K. The resonator was connected to the IMD scheme of a two-tone excitation centered with 1 MHz spacing around f_0. For LSM imaging, the device was x-y scanned by a 4 μm diameter thermal probe produced by a 1.1 μm diameter focused laser beam that is amplitude modulated with a frequency of about 100 kHz on the sample surface. Position of the LSM raster was centered not far from the peak of the standing wave current pattern near the YBCO strip edge to investigate an area with maximum $J_{HF}(x, y)$ gradient that is the most suitable for the following spatially-resolved analysis. All LSM images were acquired at T=78 K and at P_{f1}=P_{f2}=9 dBm using step-by-step scanning of the sample by the laser probe with equal distance between steps of about 0.4 μm along both x and y direction. The linear components of HF LSM $PR_f(x, y)$ were measures at f_1 and f_2 to make spatial separation between inductive $PR_X(x, y)$ and dissipative PR_R(x, y) contribution as explained by [2]. The derived $PR_X(x, y)$ was used to present LSM image of $J_{HF}(x, y)$ calibrated in real units by using a procedure described in [1]. Changes in $\delta R_s(x,y)$ were estimated as $PR_R(x,y)/PR_X(x,y)$ considering that $PR_R(x, y)$~ $J^2_{HF}(x, y)*\delta R_s(x, y)$ and $PR_R(x, y)$~ $J^2_{HF}(x, y)$.

Additionally, two LSM $PR_{2f1-f2}(x, y)$ and $PR_{2f2-f1}(x, y)$ images were measured in the same area of the resonator at combinational frequencies $2f_1$-f_2 and $2f_2$-f_1 of IMD harmonics. The spectral dependence of IMD photoresponse was estimated by using an expression for global IMD power $P_{IMD}=Q^4(P^2_{f1}P_{f2})(1/P^2_c)[1+(\Delta R/Q\Delta L)^2]$ that has been developed in [3]. Here, $P_c=2\pi fL_0I^2_{IMD}/\Delta L$ is the characteristic power, L_0 and R_0 are the linear parts, ΔL and ΔR are the nonlinearity coefficients in changes of the

inductance $L=L_0+\Delta L(I/I_{IMD})^2$ and resistance $R=R_0+\Delta R(I/I_{IMD})^2$ per unit length of the microstrip related to the case when j_{IMD} is on order of the critical current density J_c. We considered the frequency dependence of thermally induced modulation in P_{IMD} in terms of the temperature derivative $\delta P_{IMD}(f)= (dP_{IMD}/dT)\delta T$, where separate contributions from $PR_{IMD,X}(x, y)$ and $PR_{IMD,R}(x, y)$ can be deduced through partial derivatives related to f_0 and $1/Q$, correspondingly:

$$PR_{IMD} \propto \frac{\partial P_{IMD}}{\partial T} = \frac{\partial P_{IMD}}{\partial (1/Q)}\frac{\partial (1/Q)}{\partial (T)}+\frac{\partial P_{IMD}}{\partial (f_0)}\frac{\partial (f_0)}{\partial (T)} \qquad (1)$$

One can make sure that at frequencies very close to the fundamental resonance ($f \sim f_0$) dissipative and inductive components of LSM PR may be presented as:

$$PR_{IMD,R} = \frac{\partial P_{IMD}}{\partial (1/Q)} \propto \frac{-(1/Q)^3}{\left[4(f/f_0-1)^2+(1/Q)^2\right]^4} \qquad (2a)$$

$$PR_{IMD,X} = \frac{\partial P_{IMD}}{\partial (f)} \propto \frac{(1/Q)^2}{f_0}\frac{(f/f_0-1)}{\left[4(f/f_0-1)^2+(1/Q)^2\right]^4} \qquad (2b)$$

As evident from Eq. (2a), the spectrum of $PR_{IMD,R}(f)$ is approximated well by a symmetric (relative to f_0) Lorentzian-like curve of the same (negative) sign having equal magnitudes $PR_{IMD,R}(2f_1-f_2)= PR_{IMD,R}(2f_2-f_1)$ at equidistant IMD frequencies $2f_1-f_2$ and $2f_2-f_1$ around f_0. In contrast, the curve of $PR_{IMD,X}(f)$ dependence (see Eq. (2b)) crosses "0" at $f = f_0$ and has opposite signs i.e. $PR_{IMD,X}(2f_1-f_2)= (-)PR_{IMD,X}(2f_2-f_1)$ there. By virtue such an f-singularity of $PR_{IMD}(f)$, one can present LSM images of NL media as independent distributions of inductive and resistive NL sources by using the following transformations:

$$PR_{IMD,X}(x, y) = \left|\frac{PR_{IMD}(2f_1-f_2)-PR_{IMD}(2f_2-f_1)}{2}\right| \qquad (3a)$$

$$PR_{IMD,R}(x, y) = \left|\frac{PR_{IMD}(2f_1-f_2)+PR_{IMD}(2f_2-f_1)}{2}\right| \qquad (3b)$$

For the experimental verification of these statements, the same 40x20 μm^2 area of the resonator was visualized in different imaging modes of LSM contrast. In Fig. 1.
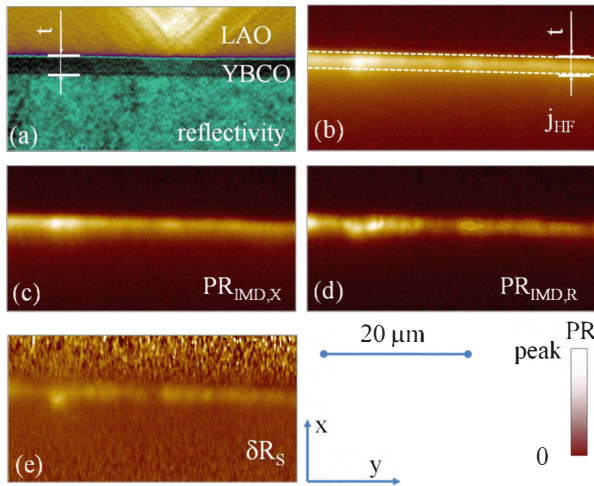

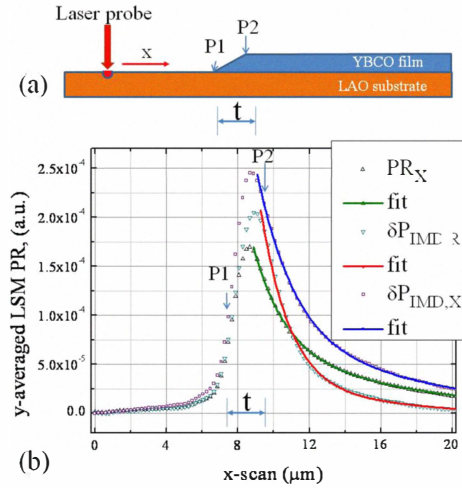Fig.1. Set of LSM images that were analyzed and discussed in the text.

Fig.2. (a) Sketch of the sample cross section along x-scan and (b) profiles of LSM response there.

In Fig. 1(a) we have pictured an optical reflectivity LSM (false-color) map of the scanned area where the surface quality of the YBCO film as well as the twinned structure of the LAO substrate is clearly visible. The YBCO strip edge has a chamfered profile producing a darker YBCO reflectivity image within a t = 4 μm strip. Top (P1 in Fig. 2(a)) and bottom (P2 in Fig. 2(a)) edges of the chamfer are placed along two dashed white lines in Fig. 2(b) where an LSM image of $J_{HF}(x, y)$ is shown. The brightest area there coincides with maximum amplitude of $J_{HF}(x, y) \sim 10^9 A/m^2$ while the darkest ones correspond to zero current density. Spatial coherence

between (i) $J_{HF}(x, y)$, nonlinear (ii) inductive $PR_{IMD,X}(x, y)$ and (iii) resistive $PR_{IMD,R}(x, y)$ components of LSM PR as well as (iv) $\delta R_s(x,y)$ is evident as one can see through comparison of all images presented in Fig. 1(b-e).

Fig. 2(b) shows typical profiles of different IMD and HF components of LSM PR(x, y = 4) together with their exponential fit that were measured along a single x-scan (see dashed line numbered as '4' in Fig. 4(a)) at fixed y(=4 lines)-cross-section. Similar profiles were used in Fig. 3 for log-log plotting of both local $PR_{IMD,R}$ and $PR_{IMD,X}$ responses as a function of local circulating HF power that can be approximated by the linear term of inductive LSM PR. As seen all four cross-sections (4, 18, 32 and 100 from Fig. 4(a)) of the resonator demonstrate a similar tendency for a linear increasing of $PR_{IMD,X}$ and square-low growth of $PR_{IMD,R}$ with respect to $PR_{HF,X}$ that is linked directly to IMD components through the same position of the laser probe. Also, the dominant contribution of $PR_{IMD,X}$ to the total IMD PR is seen at small $J_{HF}(x, y)$ closer to YBCO center. However at peak values of HF current density near the HTS film edge those amplitudes of NL response are almost equal. We believe that IMD LSM PR originates from a small laser-probe induced modulation $\delta P_{IMD}(x, y)$. of intermodulation power. In this case, $PR_{IMD,X}(x, y)$ and $PR_{IMD,R}(x, y)$ components show local NL properties of the microwave device in terms of corresponding local derivatives $\delta P_{IMD,X}(x, y)$ and $\delta P_{IMD,R}(x, y)$. Spatial integration (see Fig. 4(b)) shows that below $J_c(x, y)$ (see, for example data in Fig. 3(c) below P1), the power of real (dissipative) NL sources follows a classical cubic dependence $P_{IMD,R} \sim P^3_{IN}$ on input HF power. There were no changes in local values of the surface resistance found at all $J_{RF}(x, y) < J_c(x, y)$. Surprisingly, local sources of imaginary (inductive) IMD response show almost a square-law power dependence (see Fig. 4(b)) even below $J_c(x, y)$ except very close to $J_{RF}(x, y) \sim 0$. This contradicts previously published data considering $J_c(x, y)$ as the correct scale for the lower limit of NLs.
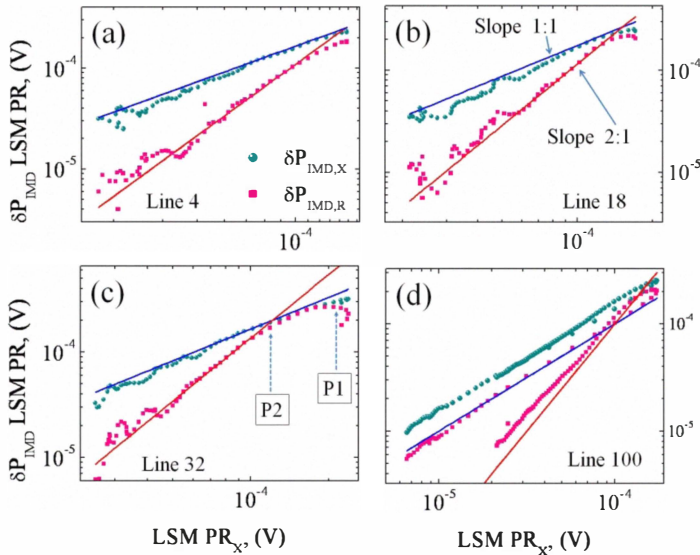

Fig.3. Log-log plots of IMD components of LSM photoresponse as a function of linear inductive one. The line cuts in parts (a) – (d) correspond to those shown in Fig. 4.
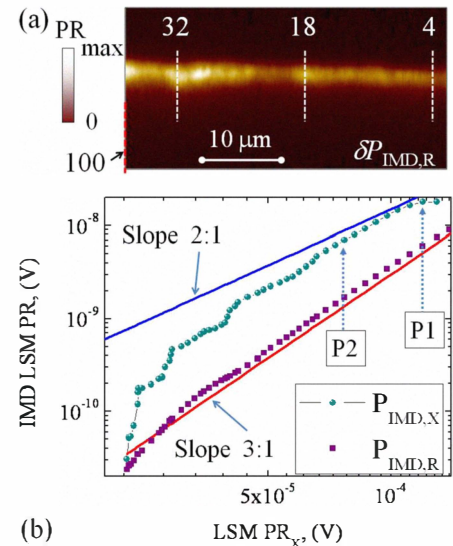
Fig.4. (a) LSM image of $PR_{IMD,R}(x, y)$ showing line-scans analyzed in Fig. 3 and (b) restored $P_{IMD}(P)$ dependencies.

References

1. A.P. Zhuravel, A.G. Sivakov, O.G. Turutanov, A.N. Omelyanchouk, S. M. Anlage, A. Lukashenko, A.V. Ustinov, D. Abraimov, "Laser scanning microscopy of HTS films and devices (Review Article)", Low Temp. Phys., Vol. 32, Issue 6, pp. 592-607, 2006.
2. A.P. Zhuravel, S.M. Anlage, A.V. Ustinov, "Measurement of local reactive and resistive photoresponse of a superconducting microwave device", Appl. Phys. Lett., Vol. 88, p. 212503, 2006.
3. T. Dahm, D J. Scalapino, B.A. Willemsen, "Phenomenological Theory of Intermodulation in HTS Resonators and Filters", Journal of Superconductivity, Vol. 12, No. 2, pp. 339-342, 1999.